AGU PUBLICATIONS

JGR

Journal of Geophysical Research: Atmospheres

RESEARCH ARTICLE

10.1002/2013JD020816

Cirrus cloud susceptibility to the injection of ice nuclei in the upper troposphere

T. Storelvmo[1] and N. Herger[2]

[1]Department of Geology and Geophysics, Yale University, New Haven, Connecticut, USA, [2]Institute for Atmospheric and Climate Science, ETH Zürich, Zürich, Switzerland

Key Points:
- Cirrus cloud seeding in the upper troposphere was simulated in CAM5
- Both cirrus cloud susceptibility and short-term climate response were analyzed
- Even globally nonuniform injection of IN leads to the desired cooling

Correspondence to:
T. Storelvmo,
trude.storelvmo@yale.edu

Citation:
Storelvmo, T., and N. Herger (2014), Cirrus cloud susceptibility to the injection of ice nuclei in the upper troposphere, *J. Geophys. Res. Atmos.*, *119*, doi:10.1002/2013JD020816.

Received 3 SEP 2013
Accepted 23 JAN 2014
Accepted article online 28 JAN 2014

Abstract Due to their net warming effect, cirrus clouds play a crucial role in the climate system. A recently proposed climate engineering mechanism (CEM) intends to reduce high cloud cover by seeding cirrus clouds with efficient ice nuclei (IN) and therefore cool climate. Here, the susceptibility of cirrus clouds to the injection of ice nuclei in the upper troposphere is investigated in the extended Community Atmospheric Model version 5 (CAM5). Due to large uncertainties associated with the dominant ice nucleation mechanism in cirrus clouds, different control cases were simulated. In addition to pure homogeneous and heterogeneous nucleation, cases with competition between homogeneous and heterogeneous nucleation and different fractions of mineral dust active as IN were considered. Whereas seeding in the pure heterogeneous case leads to a strong warming due to overseeding, an optimal seeding IN concentration of approximately 18 l^{-1} was found for the other cases. For the optimal seeding concentration, a reduction in the net cloud forcing (NCF) of up to 2 W m^{-2} was simulated, corresponding to a strong cooling effect. To optimize the cooling and minimize the amount of seeding material, globally nonuniform seeding strategies were tested, with minimal seeding in the summer hemisphere and in the tropics. With seeding applied to less than half the globe, an even stronger reduction in the NCF was achieved. This suggests that the CEM could work for an atmosphere even with considerable heterogeneous ice nucleation and that the desired cooling could be obtained without seeding the entire globe.

1. Introduction

The term *climate engineering* refers to a range of proposed methods by which Earth's climate could deliberately be altered. Such climate engineering mechanisms have recently received considerable attention, after *Crutzen* [2006] revived the topic as a means to decelerate global warming. Interestingly, one of the earliest papers mentioning climate engineering proposed it out of concerns about a new so-called "Snowball Earth" state [*Budyko*, 1969], while obviously the current focus is to identify mechanisms that could cool climate to compensate for the effect of increasing greenhouse gas concentrations. Such a climate engineering mechanism (CEM) targeting cirrus clouds was recently proposed by *Mitchell and Finnegan* [2009]. They proposed that Earth's greenhouse effect could be significantly reduced if cirrus cloud coverage in the upper troposphere (UT) was lowered.

Cirrus clouds currently cover about 30% of Earth's surface [*Rossow and Schiffer*, 1999] and play an important role in Earth's energy budget. In the shortwave part of the electromagnetic spectrum, they cool the Earth-atmosphere system by reflecting solar radiation back to space. However, this cooling does not dominate the cirrus cloud greenhouse effect; by absorbing terrestrial radiation and reemitting radiation to space at a significantly lower temperature than that of the Earth's surface, they contribute substantially to Earth's total greenhouse effect and therefore have a net warming effect [e.g., *Stephens*, 2005].

Cirrus clouds can form either by homogeneous freezing, by supercooled solution droplets freezing spontaneously, or by heterogeneous ice nucleation, with atmospheric ice nuclei (IN) aiding the phase transition. Homogeneous freezing occurs spontaneously from temperature and density fluctuations within a supercooled liquid phase, typically an aqueous sulfate droplet; its occurrence largely depends on the temperature, droplet volume, and vapor pressure [*Koop et al.*, 2000]. Generally, temperatures below about 235 K and supersaturations above 45% with respect to bulk ice are required for homogeneous freezing to occur. Laboratory studies of ice nucleation have shown that heterogeneous freezing requires lower relative humidity over ice than homogeneous freezing. Mineral dust and metallic particles have been shown to be suitable nuclei on which heterogeneous nucleation can occur [e.g., *Phillips et al.*, 2008]. However, IN concentrations

in the upper troposphere are low, and typical concentrations are in the order of 10 l^{-1} or less [*DeMott et al.*, 2003]. Measurements of relative humidity in the upper troposphere, though sparse and uncertain, often support the belief that most cirrus clouds form under conditions that are favorable for homogeneous freezing [see *Spichtinger et al.*, 2003, 2004; *Mitchell et al.*, 2011]. However, *Cziczo et al.* [2013] recently contradicted this long-held view, reporting in situ measurements of the composition of the residual particles within cirrus ice crystals after the ice was sublimated. This composition analysis, combined with relative humidity measurements, suggests that heterogeneous freezing was the dominant formation mechanism of cirrus clouds sampled in four field campaigns over North and Central America.

Our knowledge of cirrus microphysical properties largely stems from aircraft campaigns dedicated to cirrus clouds; an example is the interhemispheric differences in cirrus properties from anthropogenic emissions (INCA) campaign [*Ström et al.*, 2003; *Gayet et al.*, 2004]. In the INCA campaign, aerosol and cirrus cloud microphysical properties were measured in both hemispheres at similar latitudes during the same season, and Northern Hemisphere (NH) cirrus were found to have 20% lower relative humidity (RH) than their Southern Hemisphere (SH) counterparts. It was speculated that this interhemispheric contrast is related to corresponding contrasts in the cirrus cloud freezing threshold caused by different aerosol loadings between the two hemispheres. The SH RH values seem to be consistent with homogeneous freezing, while the NH ones suggest cirrus formation dominated by heterogeneous freezing.

It has been assumed that the success of the CEM proposed by *Mitchell and Finnegan* [2009] relied on cirrus clouds forming primarily by homogeneous nucleation in the current atmosphere. If this holds true, seeding the upper troposphere with particularly efficient IN (BiI_3 being the proposed artificial seeding material) could potentially shift the dominant nucleation mechanism from homogeneous freezing to heterogeneous nucleation. The seeding IN would form ice crystals at low supersaturations (~5%), and the ice crystals formed would grow rapidly and deplete water vapor to the extent that homogeneous ice nucleation would be suppressed. By selecting the right amount of seeding material, the goal of forming cirrus clouds containing few but large ice crystals could be achieved. The large ice crystals would have high fall velocities and therefore lead to shorter cirrus cloud lifetimes.

An initial evaluation of the viability of the CEM proposed by *Mitchell and Finnegan* [2009] was conducted by *Storelvmo et al.* [2013], who simulated the effect of adding particularly efficient ice nuclei in various concentrations to the UT region. The study showed that such a seeding could indeed produce significant cooling, sufficient to counter the entire anthropogenic contribution to the greenhouse effect since preindustrial times (approximately -2.5 W m^{-2} for an optimal seeding IN concentration of 18 l^{-1}). However, the study found that overseeding could lead to the opposite effect, i.e., a warming rather than the desired cooling. The study assumed that all cirrus clouds form homogeneously in the absence of seeding IN, an assumption that has subsequently been demonstrated not to hold. Here, we extend *Storelvmo et al.* [2013] by performing global climate simulations of the effect of cirrus seeding under a range of assumptions regarding the relative importance of homogeneous and heterogeneous nucleation in cirrus clouds in the present atmosphere. Furthermore, while *Storelvmo et al.* [2013] applied uniform seeding concentrations for the UT region of the entire globe, we here study the effect of geographically nonuniform seeding, targeting regions and seasons with the highest susceptibility. Finally, in addition to considering the effects on cirrus cloud microphysics and radiative forcings, we also address the short-term climate response that could occur after the implementation of this CEM, with a focus on land surface temperature and precipitation.

The remainder of the paper is structured as follows. Section 2 briefly describes the modeling tool and the method. Section 3 presents and discusses the results of five control simulations (subsection 3.1) and their response to spatially uniform (subsection 3.2) and nonuniform (subsection 3.3) seeding IN concentrations. Finally, our conclusions and a list of remaining open questions are given in section 4.

2. The Model and Method

The modeling tool in this study is the Community Atmosphere Model, Version 5 (CAM5), extended with parameterizations of homogeneous and heterogeneous ice nucleation by *Barahona and Nenes* [2008, 2009], hereafter BN08/09. CAM5 includes a two-moment cloud microphysics scheme described by *Morrison and Gettelman* [2008], with modifications to the ice microphysics described in *Gettelman et al.* [2010]. The aerosol treatment follows *Liu et al.* [2012a], applying the version that describes the aerosol size distribution with three log-normal modes (MAM3). One of the modes is designated for coarse mode dust particles, from

Table 1. CAM5.1 Control Cases in This Study

Case Name	Description
HOM	Pure homogeneous nucleation
HOMHET_5%	Homogeneous and heterogeneous nucleation with 5% of mineral dust active as IN
HOMHET_50%	Homogeneous and heterogeneous nucleation with 50% of mineral dust active as IN
HOMHET_100%	Homogeneous and heterogeneous nucleation with 100% of mineral dust active as IN
HET	Pure heterogeneous nucleation

which we calculate the concentration of ice nuclei available for heterogeneous ice nucleation using the BN08/09 scheme, using a semiempirical ice nucleation spectrum based on classical nucleation theory, described in BN09. As in BN09, a supersaturation of 20% was used as the freezing threshold for dust, while a freezing threshold of 5% was used for the seeding IN. Different from BN09, we assumed that soot particles do not have the ability to act as IN. Note that the choice of ice nucleation spectrum and the aerosol types active as IN in the unseeded atmosphere are likely to quantitatively affect the outcome of the study.

Cziczo et al. [2013] found that mineral dust and metallic particles dominate ice residues over Central America. This suggests that these particle types are efficient IN. The sources, properties, and atmospheric concentrations of metallic particles are currently poorly constrained and too uncertain to be incorporated in global climate simulations. We therefore only consider dust particles as natural IN in the present study. However, laboratory studies have shown that not all dust particles can act as IN [e.g., *Welti et al.*, 2009]. For the control cases of our study, we chose two cases where the fraction of mineral dust particles active as IN was limited to either 5% (HOMHET_5%) or 50% (HOMHET_50%) and one case where all the particles can act as IN (HOMHET_100%).

Additional to the control cases with competition between homogeneous and heterogeneous nucleation, the two cases of pure homogeneous (HOM) and pure heterogeneous (HET) nucleation were also considered. An overview of the control cases is given in Table 1.

For each control case, seeding series with the following uniform seeding IN concentrations in the upper troposphere were simulated: 0.1, 0.5, 1, 5, 10, 18, 25, 50, 100, and 250 IN per liter. The results of these simulations are presented in subsection 3.2. In order to achieve an optimal seeding strategy, nonuniform seeding simulations were conducted for all control cases except for HET. These results are presented and discussed in subsection 3.3.

All the simulations were run for 5 years, and the means of the last 4 years were used in the analysis. Simulations were run with climatological sea surface temperatures and anthropogenic aerosol emissions following *Lamarque et al.* [2010], while dust emissions follow *Mahowald et al.* [2006]. All simulations were run with a finite volume dynamical core, a resolution of 1.9° latitude and 2.5° longitude and 30 vertical levels.

3. Results/Discussion

3.1. Control Cases

Table 2 shows the comparison between the global and annual mean of the control cases of this study and satellite observation data (OBS). It is evident that the case with pure heterogeneous nucleation (HET) is furthest away from the observations. The other control cases can all be considered to be reasonably realistic.

Table 2. Simulated Global and Annual Mean Cloud Cover (CC), Ice Water Path (IWP), Liquid Water Path (LWP), Net Cloud Forcing (NCF), Shortwave Cloud Forcing (SWCF), and Longwave Cloud Forcing (LWCF) From the CAM5.1 As Well As From Satellite Observations (OBS)[a]

Case Name	CC (%)	IWP (g m^{-2})	LWP (g m^{-2})	NCF (W m^{-2})	SWCF (W m^{-2})	LWCF (W m^{-2})
HOM	68.3±0.17	21.6±0.07	47.0±0.27	−26.5±0.15	−60.2±0.13	33.7±0.08
HOMHET_5%	68.3±0.15	21.6±0.08	47.0±0.14	−26.5±0.25	−60.0±0.11	33.6±0.19
HOMHET_50%	68.3±0.12	21.2±0.14	46.9±0.06	−26.7±0.15	−59.6±0.14	32.9±0.07
HOMHET_100%	68.0±0.16	21.0±0.05	47.0±0.30	−26.9±0.29	−59.4±0.31	32.5±0.08
HET	61.4±0.17	15.8±0.12	43.7±0.14	−29.4±0.20	−49.2±0.15	19.8±0.14
OBS	~ 67	20–70	30–50	−23.8 to −17.2	−50.5 to −44.5	22.4–30.4

[a]Observations are taken from ISCCP [*Rossow and Schiffer*, 1999] (CC), a combination of CloudSat and CALIPSO retrievals (IWP, LWP), from ERBE and CERES (NCF), and from *Stephens et al.* [2012] (SWCF, LWCF).

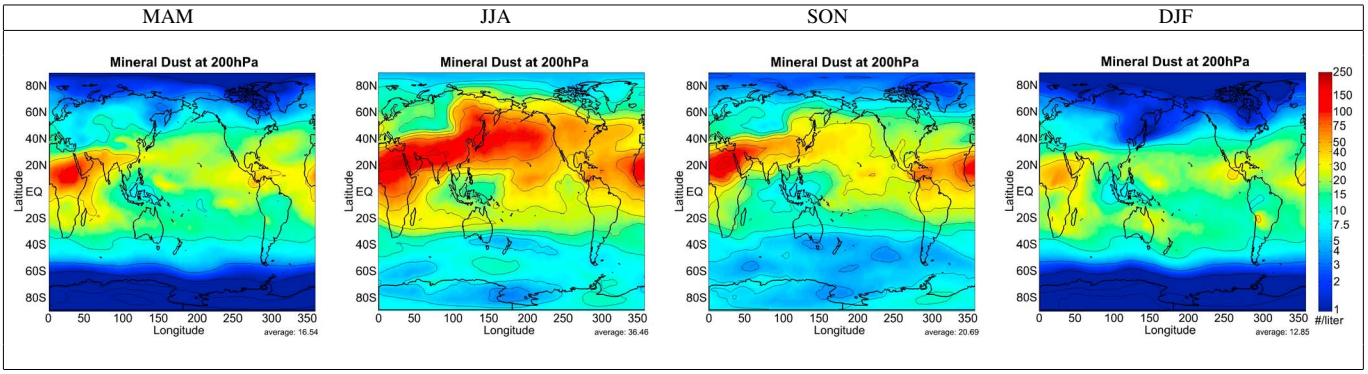

Figure 1. Seasonal number concentrations of mineral dust at the 200 hPa level for the 4 year mean of the HOM case. A logarithmic color scale is used to represent the number concentrations. MAM: March, April, and May; JJA: June, July, and August; SON: September, October, and November; DJF: December, January, and February.

However, the modeled net cloud forcing (NCF) is generally too low due to deviations in the shortwave cloud forcing (SWCF). The control cases change in an overall systematic manner when the percentages of mineral dust active as IN are changed.

Figure 1 shows the geographical and seasonal distribution of the number concentration of mineral dust in the coarse mode at the 200 hPa level using a logarithmic scale. There are no big differences between the control cases, so only the maps of the HOM case are shown here. At this level, the highest concentrations can be found in NH summer (JJA) and fall (SON). However, note that in the lower troposphere, the simulated dust concentrations peak in spring, in agreement with findings reported in *Yu et al.* [2012]. The Saharan desert and Asian dust have the highest contribution to mineral dust in the atmosphere. *Prospero et al.* [2002] found a similar seasonal and spatial variability in mineral dust emissions.

Under consideration of results from the INCA (Interhemispheric Differences in Cirrus Properties From Anthropogenic Emissions) field experiment, *Haag et al.* [2003] suggested that cirrus clouds in the SH midlatitudes are dominated by homogeneous nucleation. In contrast, cirrus clouds in the NH are formed by a combination of homogeneous and heterogeneous nucleation. The modeling study of *Liu et al.* [2012b] lead to similar results as they suggested that the contribution of homogeneous nucleation to the in-cloud ice crystal number concentration is high in the upper troposphere in the tropics and in the SH. The simulated in-cloud ice crystal number concentrations and effective radii for three of the control cases (HOM, HOMHET_50%, and HET) are shown in Figure 2. Ice crystal number concentrations and sizes are similar in HOM and HOMHET_50%, suggesting that the concentration of mineral dust IN is often too low for homogeneous ice nucleation to be suppressed. In agreement with the previous studies, these simulations produce maxima in ice crystal number concentrations in the SH upper troposphere. In contrast, simulation HET produces much lower ice crystal number concentrations that have maxima in the midlatitude storm tracks in the lower/middle troposphere. As a consequence of the lower ice crystal number concentrations, ice crystals in the upper troposphere are also much larger in simulation HET, as expected.

Our simulations agree with the findings of *Liu et al.* [2012b] in the sense that a high number concentration of heterogeneous IN in the NH midlatitudes can be assigned to the main dust sources in North African and Asian deserts. Therefore, the heterogeneous nucleation mechanism is expected to be important in the NH, particularly in regions with more mineral dust available. This is confirmed by Figure 3, which displays the fraction of ice crystals that were formed heterogeneously (HETFRAC) on the 200 hPa level, where cirrus clouds can be found. A HETFRAC of 1, as seen in the HET control case (Figure 3e), indicates that all the ice crystals were formed heterogeneously, whereas HETFRAC equals 0 in the HOM case (Figure 3a). HETFRAC features large seasonal variations, mainly caused by temperature changes and changes in mineral dust concentration. As HETFRAC is highest in NH summer (JJA) and fall (SON), cirrus clouds are expected to have the weakest susceptibility to additional seeding then. However, even in the HOMHET_100% case where all the mineral dust particles can act as IN, the heterogeneous IN concentration is still not high enough in order to completely suppress homogeneous freezing.

A comparison to the field campaigns which built the basis for the paper of *Cziczo et al.* [2013], combined with the knowledge that it is unlikely that all dust particles have the ability to act as IN, leads to the

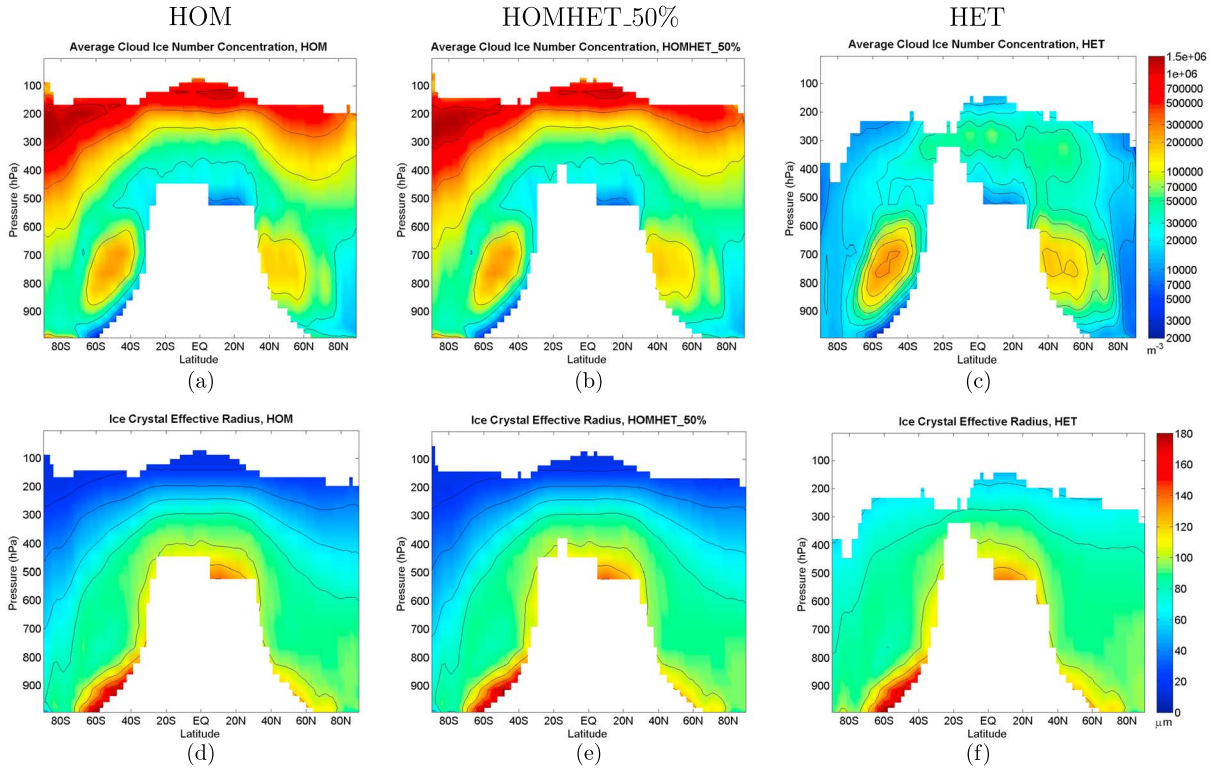

Figure 2. Zonal mean in-cloud ice crystal number concentrations and effective radii: (a and d) HOM, (b and e) HOMHET_50%, and (c and f) HET. A logarithmic color scale is used to represent the number concentrations.

assumption that the HOMHET_50% control case (Figure 3c) is closest to reality. The four aircraft campaigns (MACPEX, CRAVE, TC4, and CRYSTAL-FACE) were conducted in different seasons mostly over Central and North America (flight tracks included in Figure 3c). In 94% of cloud encounters, the ice crystals appeared to have formed by heterogeneous nucleation [*Cziczo et al.*, 2013]. However, the cirrus encounters represented both convective outflow and synoptically formed cirrus clouds. Only the latter is relevant for the comparison with Figure 3. All in all, we conclude that the HOMHET_50% control case stands in good agreement with these observations.

3.2. Uniform Seeding

Based on the five control cases, seeding scenarios with different uniform seeding IN concentrations (0.1, 0.5, 1, 5, 10, 18, 25, 50, 100, and 250 IN per liter) were analyzed. The seeding IN were introduced into the upper troposphere for temperatures below 235 K, and they were all assumed to have the ability to act as IN. Figure 4 shows the changes between the seeded cases with different IN concentrations and the control cases. The HOM case and the cases with competition between homogeneous and heterogeneous nucleation behave in a systematic way with HOM as the case with the largest sensitivity to seeding and decreasing effects with increasing percentages of mineral dust active as IN. For the pure heterogeneous case, an overseeding as described by *Storelvmo et al.* [2013] can be observed. As evident from Table 2, the HET case differs dramatically from the other four control cases and also responds very differently to seeding.

For the other control cases, no significant changes can be observed up to a seeding concentration of approximately 1 IN per liter. With increased seeding, the cloud ice number concentration (Figure 4a) begins to decrease and the ice crystal effective radius (Figure 4b) is increased correspondingly. This leads to fewer and larger ice crystals which effectively sediment out due to their higher fall speed. As a direct result thereof, the high cloud cover (Figure 4c) is decreased, with associated reduction in the ice water path (Figure 4d). Seeding of cirrus clouds also impacts the radiative properties of the clouds. With decreased high cloud cover, less longwave radiation is trapped in the atmosphere. This reduced greenhouse effect of the cirrus clouds leads to a decrease in longwave cloud forcing (LWCF) (Figure 4e) and therefore a cooling of the climate. The optically thinner clouds are characterized by a decreased albedo which allows more solar

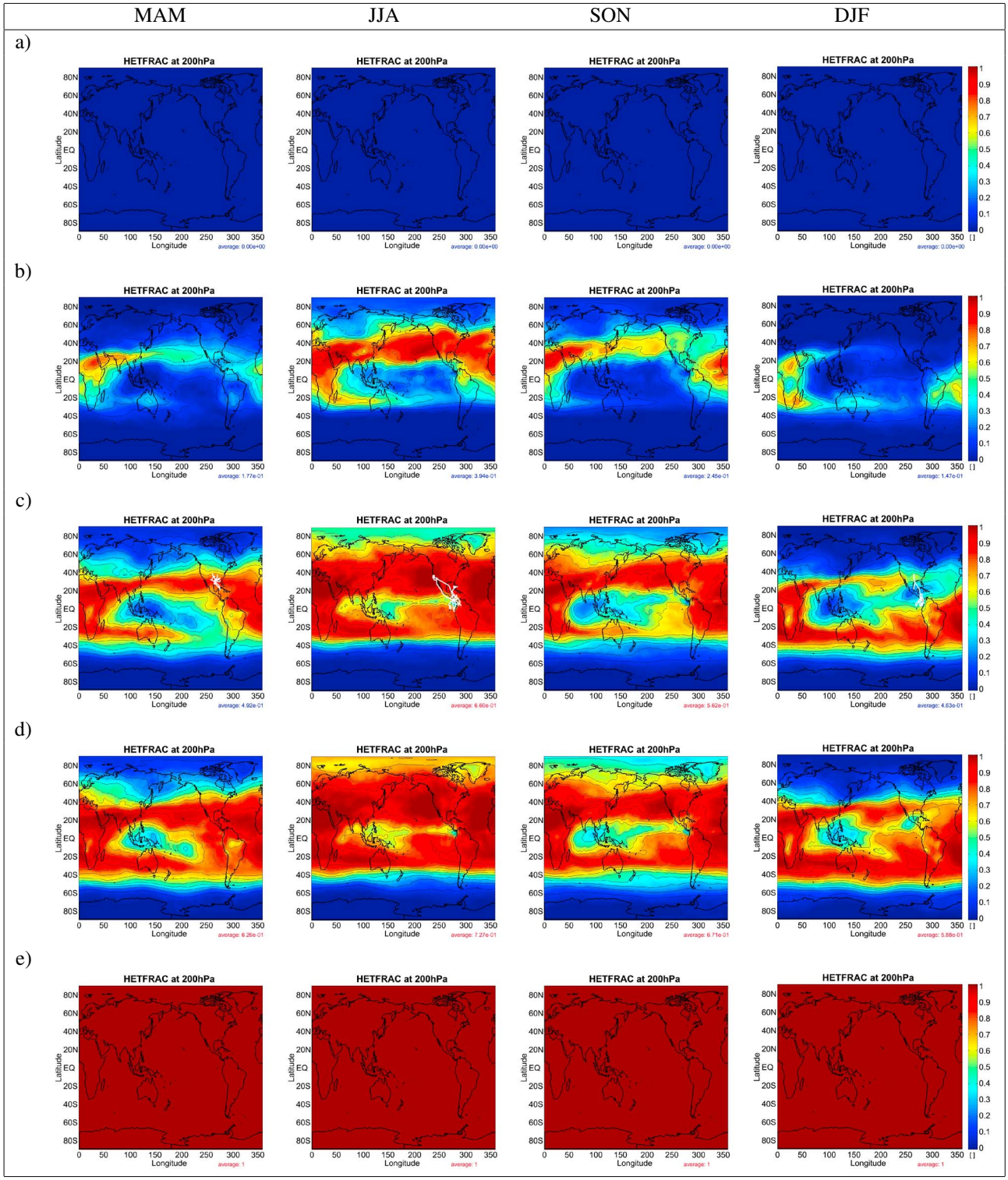

Figure 3. Maps of the fraction of ice crystals that is formed heterogeneously (HETFRAC) at 200 hPa for the 4 year means of the different seasons in columns and control cases in rows. The following control cases are displayed: (a) HOM, (b) HOMHET_5%, (c) HOMHET_50%, (d) HOMHET_100%, and (e) HET. MAM: March, April, and May; JJA: June, July, and August; SON: September, October, and November; DJF: December, January, and February. The flight tracks of the *Cziczo et al.* [2013] field campaigns are shown on the HOMHET_50% plots for the corresponding seasons. The globally averaged values in HETFRAC are given beneath the corresponding plots.

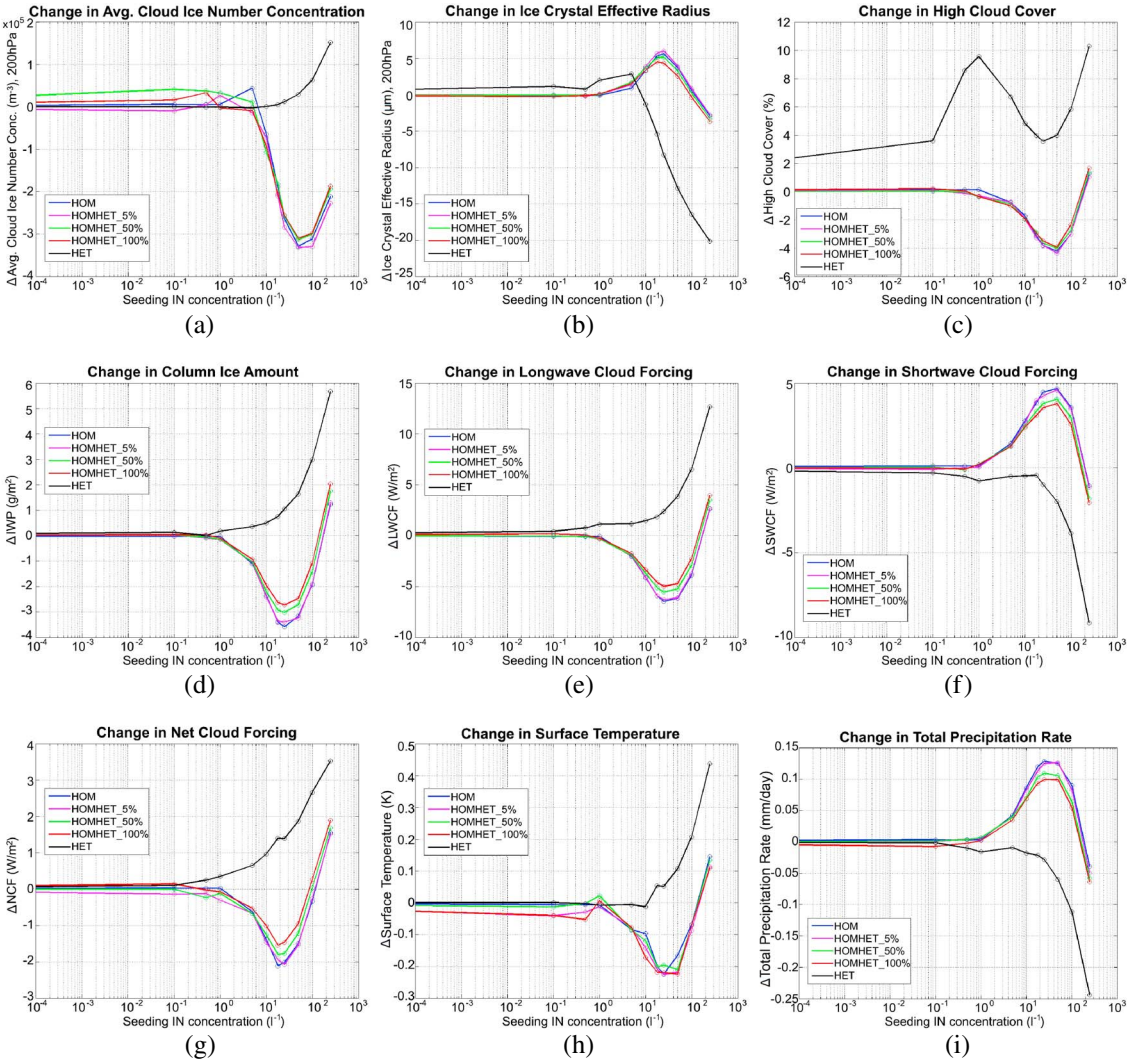

Figure 4. Curves of the 4 year global means for the difference between the seeding and five control simulations. The plots are showing the following as a function of seeding IN concentration: (a) average in-cloud ice number concentration at 200 hPa, (b) ice crystal effective radius at 200 hPa, (c) high cloud cover, (d) column ice amount (IWP), (e) longwave cloud forcing (LWCF), (f) shortwave cloud forcing (SWCF), (g) net cloud forcing (NCF), (h) surface temperature, and (i) total precipitation.

radiation to enter Earth's atmosphere and reach the ground. The shortwave cloud forcing (SWCF) (Figure 4f) partially compensates the cooling caused by the reduction in LWCF. The net cloud forcing (Figure 4g) shows that the reduced LWCF dominates over the increase in SWCF and a cooling of the atmosphere results. Only a small reduction in surface temperature (Figure 4h) around −0.2 K can be observed as we do not allow the ocean to change its temperature. As a consequence of the reduced atmospheric temperature and constant sea surface temperature, the total precipitation rate (Figure 4i) is increased. The change in total precipitation is dominated by the change in convective precipitation (not shown here).

The above mentioned direct and indirect effects of seeding cirrus clouds are not valid for the HET control case. Even for small seeding IN concentrations, all the ice crystals are formed by heterogeneous nucleation. With additional IN, we enter the overseeding regime with increased cloud ice number concentrations and dramatically decreased ice crystal effective radius [*Storelvmo et al.*, 2013]. An interesting behavior can be found for the high cloud cover in the HET case (Figure 4c). The S-shaped curve can be explained as a competition between changes in temperature and ice crystal number concentration. Between 0.1 and 1 seeding IN per liter, a dramatic increase in high cloud cover of almost 10% can be observed as we keep more ice crystals in the atmosphere. A warming signal in the atmospheric temperature can be found in the same region (not shown here). For seeding concentrations between 1 and 25 IN per liter, the high cloud cover decreases rapidly. We find a strong increase in atmospheric temperature with decrease in both relative and specific

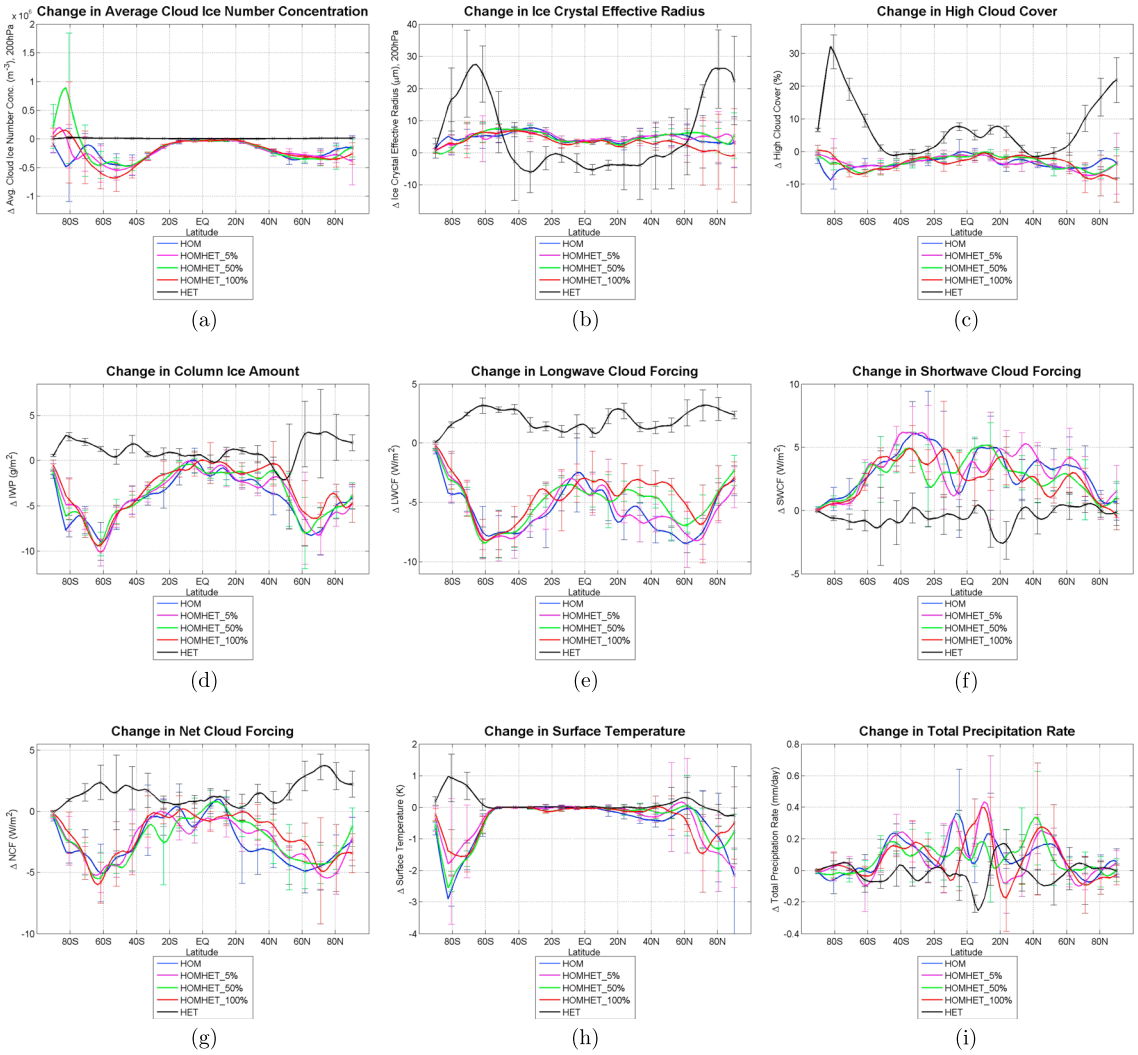

Figure 5. Zonal mean plots for the 4 year means for the difference between the seeding and five control cases showing changes in the following variables due to an optimal seeding of 18 IN per liter: (a) average in-cloud ice number concentration at 200 hPa, (b) ice crystal effective radius at 200 hPa, (c) high cloud cover, (d) column ice amount (IWP), (e) longwave cloud forcing (LWCF), (f) shortwave cloud forcing (SWCF), (g) net cloud forcing (NCF), (h) surface temperature, and (i) total precipitation. The curves represent moving averages, and the error bars show the standard deviation.

humidity in this region. Moreover, the ice crystal effective radius is slightly increased. With seeding concentrations higher than 25 IN per liter, the curve of the high cloud cover continues to rise as it did for smaller seeding IN concentrations. It goes hand in hand with an increase in atmospheric and surface temperature, relative and specific humidity (more water vapor available), and cloud ice number concentration. The other curves for the HET case behave as expected.

Apart from HET, all the control runs feature an optimum at the same seeding IN concentration. This optimal seeding IN concentration depends on the variable that is considered. The change in net cloud forcing (NCF) (Figure 4g) features an optimum with up to $-2\,\mathrm{W\,m^{-2}}$ at 18 seeding IN per liter for all control cases except HET and is hereafter referred to as the optimal seeding IN concentration. It is important to note that this optimal seeding IN concentration is sensitive to the model treatment of subgrid-scale vertical velocity and associated cooling rates [*Storelvmo et al.*, 2013].

Zonal mean plots showing the difference between the various control cases (HOM, HOMHET_5%, HOMHET_50%, HOMHET_100%, and HET) and the corresponding simulations with an optimal seeding of 18 IN per liter are shown in Figure 5. The additional IN outcompetes homogeneous nucleation, which then leads to fewer but larger ice crystals. This effect can be seen in Figures 5a and 5b. The strongest increase in ice crystal effective radius can be observed in high latitudes where the ice water path (Figure 5d) features a

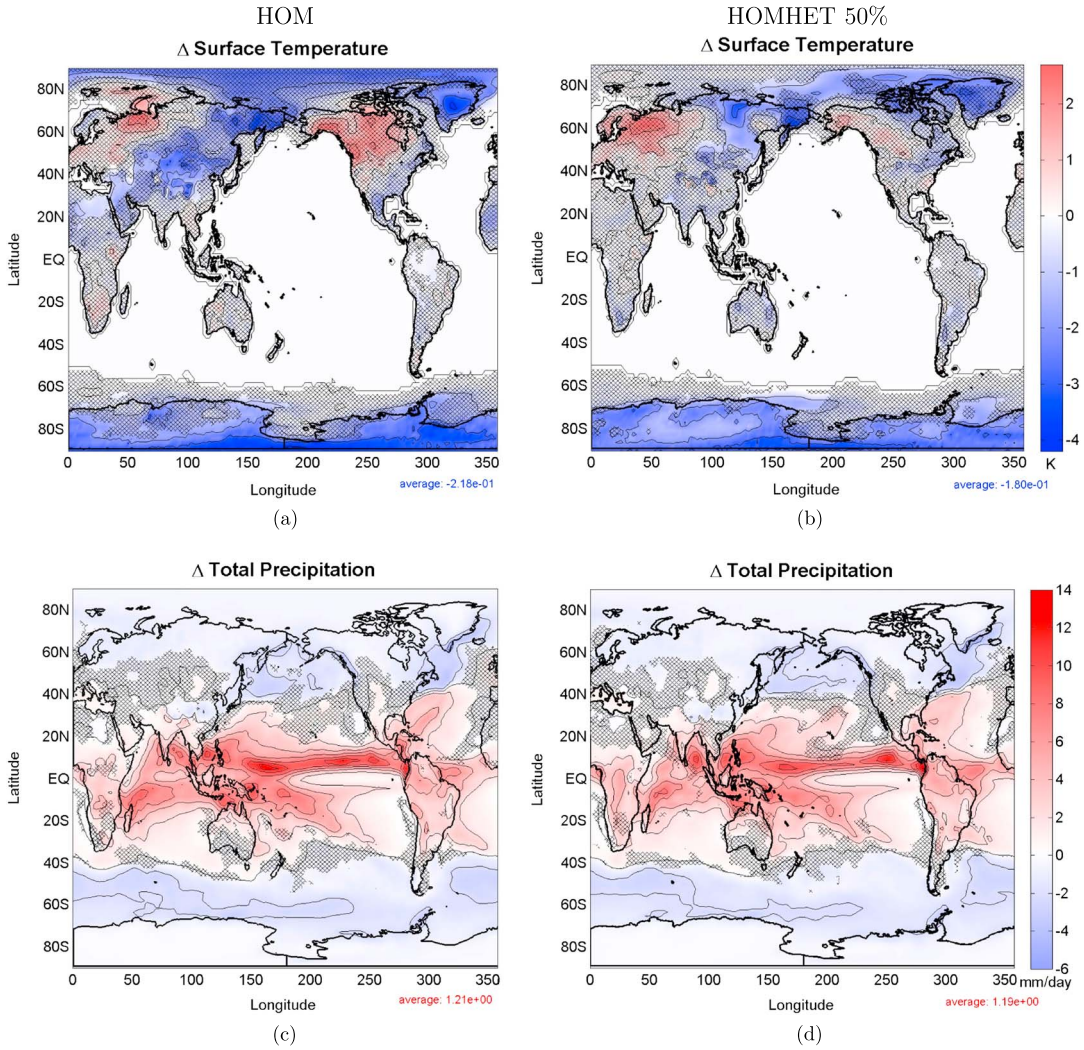

Figure 6. Maps of the 4 year mean showing the effect of optimal seeding with 18 IN per liter for the HOM case and the HOMHET_50% case for the following variables: (a and b) surface temperature and (c and d) total precipitation. The globally averaged changes in the variables are given beneath the corresponding plots. The hatching indicates regions where the difference between the seeding and control simulation was not statistically significant (paired *t* test with a significance level of 5% was applied).

minimum due to higher fall speeds. The pure heterogeneous control case leads to a strong increase in high cloud cover (Figure 5c) and therefore warming in most of the regions (Figure 5h). Big variations between the different control cases can be observed in the Northern Hemisphere due to the strong dependency on mineral dust concentration.

One of the objectives of removing cirrus clouds is to reduce the LWCF (Figure 5e) and keep the shortwave cloud forcing at a minimum (Figure 5f). The net cloud forcing (Figure 5g) for the HET case is increased which leads to a warming. For all the other control cases with optimal seeding of 18 IN per liter, the LWCF dominates the SWCF and this leads to the desired cooling of the climate. Note, however, that in the tropics the net cloud forcing remains unchanged or is even increased. The same is true for the midlatitudes of the summer hemisphere (not shown). This effect is undesired, as seeding in these regions would have negligible effect and could even lead to a warming. This is a result of an almost perfect cancelation between changes in LWCF and SWCF in these regions, which can be explained as follows: Changes in ice crystal number concentrations and sizes, as well as in ice water path and cloud cover, are small in the tropics. This is partly because HETFRAC is already relatively high there (cf. Figure 3), meaning that cirrus susceptibility to IN injection is small in this region. Furthermore, cirrus clouds in the tropics are formed mainly by convective outflow, a process which is not affected by the IN injection in the model. Finally, despite the small changes in the cloud

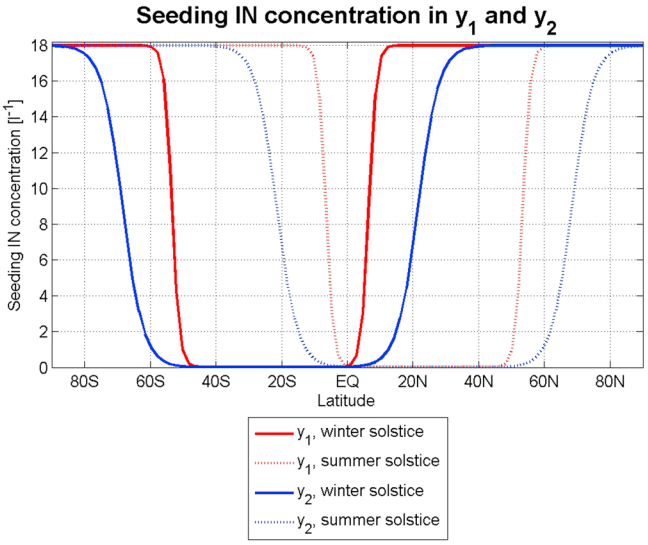

Figure 7. Seeding IN concentrations for the two nonuniform seeding strategies (y_1 and y_2, in l^{-1}) as a function of latitude.

properties, the reduction in the magnitude of the SWCF is relatively strong in the tropics. This is the result of the sun being directly overhead, so that even a small reduction in cloud albedo may reduce the SWCF significantly. In subsection 3.3, this insight is taken into account in order to create an optimal nonuniform seeding strategy.

The strongest surface temperature decrease can be observed in the Southern Hemisphere where HETFRAC is lowest (cf. Figures 5h and 3). The main dust sources can be found in the Northern Hemisphere, where a weaker cooling due to a larger initial HETFRAC is achieved.

This climate engineering technique also leads to changes in the precipitation through various so-called fast feedback mechanisms [*Zelinka et al.*, 2013]. These are feedbacks in response to the cooling of the land surface and the atmosphere, combined with a sea surface which is kept at climatological temperatures. This can be thought of as the short-term climate response one would observe after the introduction of this CEM, because the land surface and atmospheric temperatures respond more rapidly to an imposed forcing than does the sea surface temperature. An increase in total precipitation with peaks in the tropics and midlatitudes can be observed (Figure 5i). The convective precipitation dominates as the changes in large-scale precipitation are up to an order of magnitude smaller (not shown here).

Maps showing the effect of optimal uniform seeding of 18 IN per liter are displayed in Figure 6. The left column shows changes in surface temperature and total precipitation (convective and large scale) in the HOM case. The same is displayed in the right column for the HOMHET_50% case.

As we force the ocean temperature to remain unchanged, only temperature changes over the continents can be observed (Figures 6a and 6b) and are often not statistically significant (indicated by hatching). The cooling effect is strongest in high latitudes. While some regions experience a warming, these changes were not statistically significant at the 95% confidence level. A general intensification of the extratropical cyclones and a strengthening of the trade winds were observed (not shown) and are expected when the temperature gradient between low and high latitudes is increased. The increased equatorward flow is the surface manifestation of a strengthening of the Hadley cell, a tropical atmospheric circulation that is responsible for the heat transport from the tropics to the midlatitudes. This is also expected when the temperature gradients between equator and the poles are increased. As expected, the globally averaged surface temperature decrease is smaller in the HOMHET_50% case (Figure 6b) than in the HOM case.

An overall increase in total precipitation rate (Figures 6c and 6d) can be observed. The biggest changes can be found in the intertropical convergence zone (ITCZ). Increased equatorward flow and low-level convergence leads to stronger convection and hence increased convective precipitation there. An increase in precipitation is also evident in the midlatitude storm tracks, particularly over the ocean. This is a response to the cooler atmosphere and an ocean surface which is kept at higher temperatures. This leads to a stronger temperature gradient and thus a higher evaporation rate and stronger convection.

3.3. Nonuniform Seeding

Based on the results discussed in subsection 3.2, it is evident that seeding in the tropics should be avoided as it leads to negligible changes or even an increase in NCF (cf. Figure 5g) and could therefore lead to a warming. Moreover, in order to minimize the amount of seeding IN, the climate engineering mechanism should not be applied in the summer hemisphere as the smallest cooling effects are expected in this season. This is especially true for the NH, where the combined effect of large HETFRAC values and maximum solar

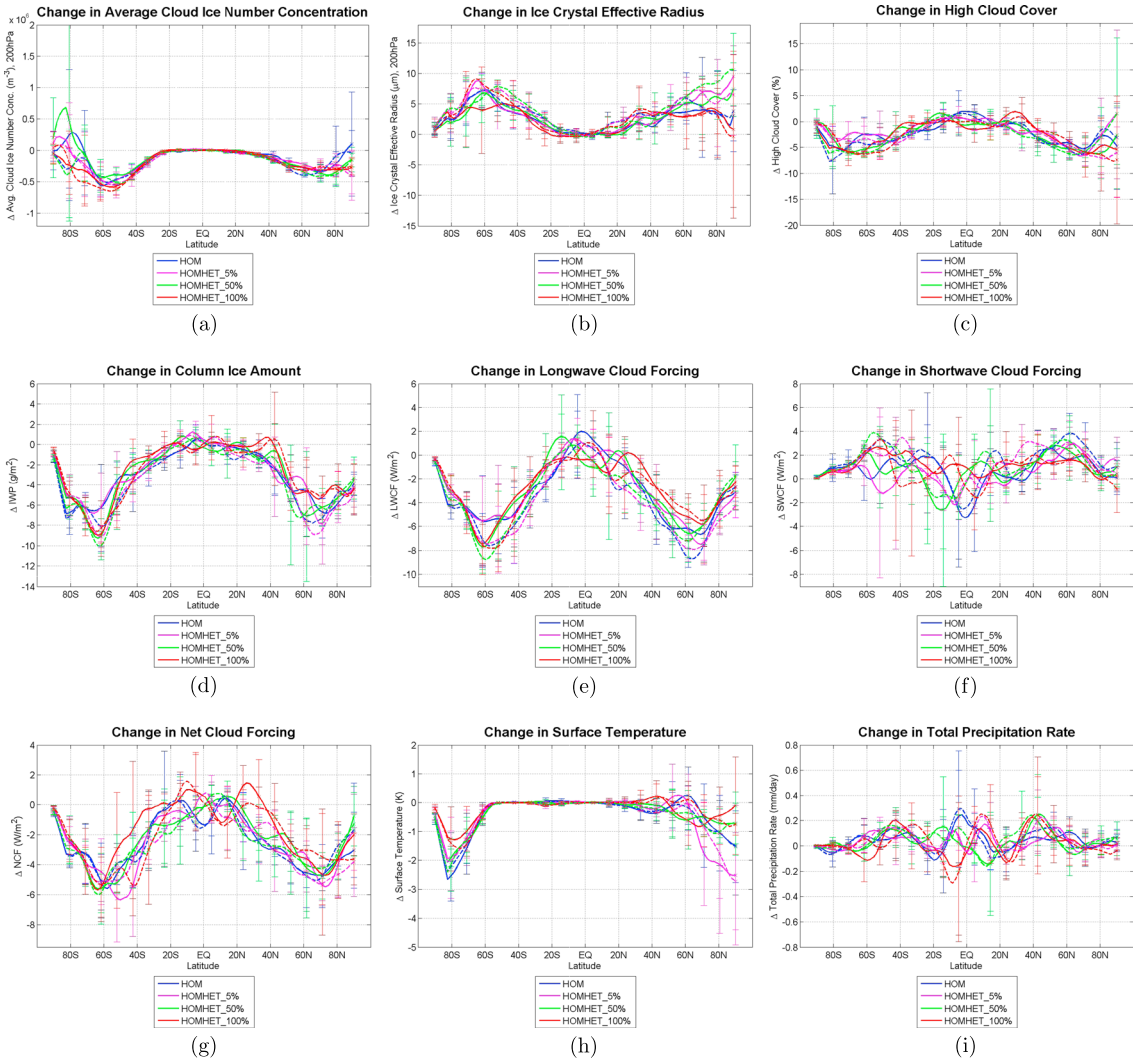

Figure 8. Zonal mean plots for the 4 year means of the difference between the seeding and control cases showing changes in the following variables due to a nonuniform seeding: (a) average in-cloud ice number concentration at 200 hPa, (b) ice crystal effective radius at 200 hPa, (c) high cloud cover, (d) column ice amount (IWP), (e) longwave cloud forcing (LWCF), (f) shortwave cloud forcing (SWCF), (g) net cloud forcing (NCF), (h) surface temperature, and (i) total precipitation. The solid (dashed) lines correspond to the nonuniform seeding based on the function y_2 (y_1). The curves represent moving averages, and the error bars show the standard deviation.

insolation lead to relatively small changes in LWCF that are largely canceled by the corresponding changes in SWCF.

Two nonuniform seeding methods were tested in the context of this study in order to keep the seeding IN amount as small as possible and to optimize the cooling effect. The following combined logistic equations as a function of the solar noon zenith angle θ_s were tested:

$$y_1 = -\frac{18}{1 + exp(-50 \cdot (\theta_s + \pi/6))} + 18 + \frac{18}{1 + exp(-50 \cdot (\theta_s - \pi/6))} \quad (1)$$

$$y_2 = -\frac{18}{1 + exp(-18 \cdot (\theta_s + \pi/4))} + 18 + \frac{18}{1 + exp(-18 \cdot (\theta_s - \pi/4))} \quad (2)$$

where y_1 and y_2 are the seeding IN concentrations (in l^{-1}), shown for the two solstices in Figure 7. The equations describe a seeding strategy where the seeding concentration is maximal (18 seeding IN per liter) for large zenith angles and therefore low altitudes of the sun. Using the solar noon zenith angle as independent variable, we found a way to maximize the seeding amount in the high latitudes and avoid seeding in the tropics. The transition between these two extremes is smooth.

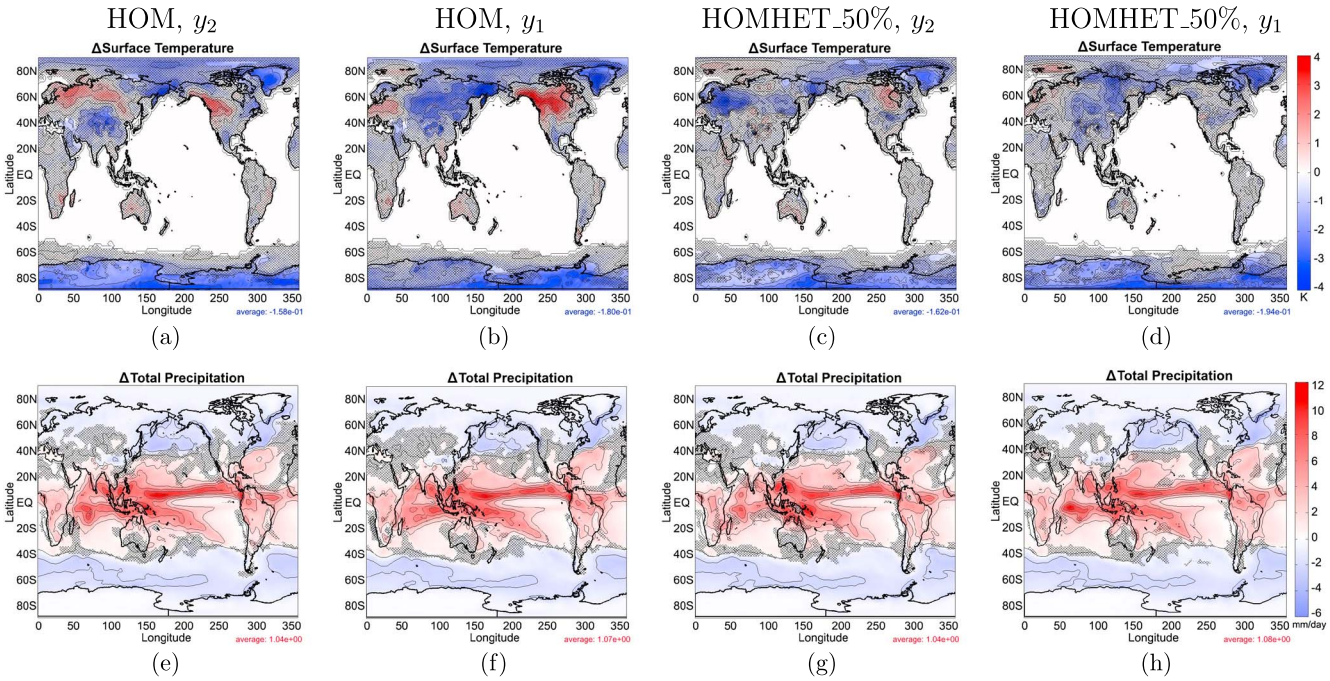

Figure 9. Maps of the 4 year means showing the effect of nonuniform seeding for the HOM case and the HOMHET_50% case. HOM with y_2, HOM with y_1, HOMHET_50% with y_2, and HOMHET_50% with y_1. Plots are shown for the following variables: (a–d) surface temperature and (e–h) total precipitation rate. The globally averaged changes in the variables are given beneath the corresponding plots. The hatching indicates regions where the difference between the seeding and control simulation was not statistically significant (paired *t* test with a significance level of 5% was applied).

Equation (1) describes a nonuniform seeding where approximately 40% of the Earth's surface is seeded at any given time. The seeding occurs from the poles down to latitudes close to the tropics where the seeding material is assumed to be inefficiently transported to the equator by diffusion. In the height where the seeding occurs, the Hadley cell is directed toward higher latitudes. Therefore, the transport to the equator is inhibited and the seeding IN concentration decreases quickly.

Equation (2) corresponds to a strategy where only approximately 15% of Earth's surface is seeded at any given time. The seeding is confined to high latitudes, and the seeding material is afterward efficiently transported to lower latitudes through baroclinic waves. Due to the efficient mixing, the transition from the poles to the equator is smoother as compared to the nonuniform seeding described by equation (1).

Figure 8 displays the zonal mean differences between the control simulations (except from simulation HET) and the two corresponding nonuniform seeding simulations. The dashed curves correspond to a seeding with equation (1) as underlying function. The solid curves result from a seeding strategy described by equation (2). The curves are comparable to Figure 5, and it is noticeable that almost the same net cloud forcing (Figure 6g) is achieved with less seeding material.

As mentioned above, the seeding strategy with equation (1) covers a greater percentage of Earth's surface as compared to equation (2). With a higher seeding IN concentration, the effect of seeding is greater in most of the variables shown in Figure 8.

Considering that a nonuniform seeding strategy with less seeding IN required leads to very similar results as the uniform seeding of 18 per liter globally indicates that there is a big potential for saving seeding material and effort and still having the desired effects.

Figure 9 shows maps of changes in surface temperature and precipitation due to the two kinds of nonuniform seeding for the HOM and HOMHET_50% control cases. From left to right, the columns show the following: HOM with y_2, HOM with y_1, HOMHET_50% with y_2, and HOMHET_50% with y_1.

As expected, we find larger sensitivities in the HOM case than in the HOMHET_50% case. The spatial patterns of changes in the surface temperature are very diverse for the different cases, but they all have in common that the statistically robust feature is a cooling of high latitude land regions.

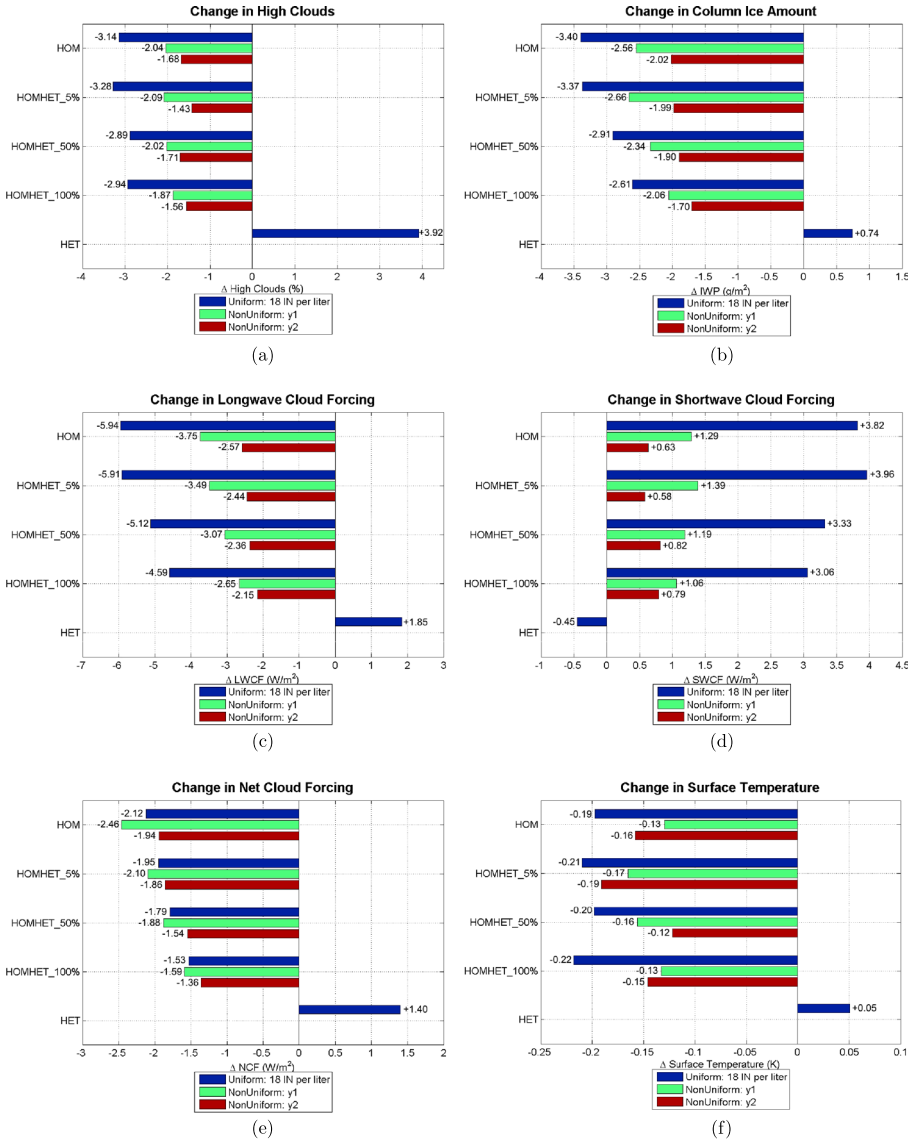

Figure 10. Comparison of the effect of optimal uniform (18 IN per liter) and nonuniform seeding (y_1 and y_2) in the control cases. Changes in (a) high cloud cover, (b) column ice amount (IWP), (c) longwave cloud forcing, (d) shortwave cloud forcing, (e) net cloud forcing, and (f) surface temperature are shown. For the HET case, only the uniform seeding with 18 seeding IN per liter was simulated. Values are based on 4 year global means.

Figure 10 shows bar plots of the effect of optimal uniform (18 IN per liter) and nonuniform seeding (equations (1) and (2)) in the control cases. As expected, the cirrus clouds are most sensitive when the uniform seeding strategy, where the whole globe is seeded, is applied. As the HET case never leads to the desired cooling effect of the climate, the nonuniform seeding simulations were not conducted for this case. The behavior is systematic as the effect of seeding seems to decrease with decreasing seeding IN concentration for most of the variables.

The nonuniform seeding with equation (1) as underlying function achieves in most cases greater effects as compared to the function in equation (2) where less area of Earth's surface is seeded. The behavior in surface temperature (Figure 10f) deviates from this statement as it is a result of a combination of the direct radiative effect of increased seeding IN and more complex feedback mechanisms.

It is noticeable that the two nonuniform seeding strategies perturb the longwave (Figure 10c) and shortwave cloud forcing (Figure 10d) in a much smaller degree as compared to the uniformly seeded scenarios. The nonuniform seeding based on y_1 leads to an even larger decrease in net cloud forcing (Figure 10e) than

the uniform seeding. This feature shows that there is no need to seed the whole globe to induce a cooling effect and even in the case with 100% of mineral dust active as IN the climate engineering mechanism still leads to the desired cooling.

4. Conclusions

The aim of this study was to investigate the susceptibility of cirrus clouds to the injection of ice nuclei (IN) in the upper troposphere. The extended CAM5 with parameterizations of homogeneous and heterogeneous ice nucleation by *Barahona and Nenes* [2008, 2009] was used to simulate control cases with different ice crystal formation mechanisms, fractions of mineral dust active as IN, and corresponding seeding strategies with different seeding IN concentrations. The long-held assumption that cirrus clouds are mainly formed homogeneously seems no longer to be valid, as *Cziczo et al.* [2013] suggested that heterogeneous nucleation is the main formation mechanism of ice crystals based on four field campaigns conducted over Central and North America. In order to consider these newest findings, the pure homogeneous and heterogeneous case and competition between them were simulated.

The comparison of the fraction of ice crystals that were formed heterogeneously between the field campaigns analyzed by *Cziczo et al.* [2013] and our simulations leads to the conclusion that the case where 50% of mineral dust can act as IN and competition between homogeneous and heterogeneous nucleation is allowed yields the best agreement with observations without making the unrealistic assumption that all dust particles can act as IN.

The control case with pure heterogeneous nucleation turned out to belong to the overseeding regime as defined by *Storelvmo et al.* [2013] as seeding leads to an increase in high cloud cover and therefore a warming of the climate. In contrast, an optimal seeding concentration of 18 IN per liter was found for the other control cases with a reduction in the net cloud forcing of up to 2 W m^{-2}. This is achieved by a reduction in cloud ice number concentration and increase in ice crystal effective radius. The fewer but larger ice crystals sediment out efficiently due to their higher fall speed and reduce the column ice amount and therefore the high cloud cover. As the longwave cloud forcing (greenhouse effect of cirrus clouds) is reduced to a greater extent as compared to the increase in shortwave cloud forcing (decrease in cloud albedo), a cooling in surface temperature results. The resulting cooling of the surface of approximately −0.2 K is moderate as the sea surface temperature is kept at climatological temperatures while the atmosphere and land surfaces were cooled down. This model setup therefore reflects the short-term climate response to seeding as the land atmosphere is thought to react much faster to changed radiative forcings as compared to the ocean. Through feedback mechanisms, an increase in total precipitation (mainly in the ITCZ) can be observed.

Zonal mean plots of the effect of optimal seeding allow for identification of seeding strategies where the seeding material can be minimized and the net cloud forcing optimized. Seeding in the summer hemisphere and the tropics turned out to be undesired as the effect of seeding is smallest there and would sometimes even lead to a warming. Two globally nonuniform seeding strategies with different fractions of the Earth's surface seeded at any given day of the year were analyzed with respect to changes in radiative forcings and cirrus cloud susceptibility. Surprisingly, for the nonuniform seeding strategy where the CEM was applied over approximately 40% of the globe's surface, an even greater reduction in NCF as compared to uniform seeding in the pure homogeneous case could be achieved. The finding that this CEM can lead to the desired cooling with only half the globe seeded and large fractions of mineral dust active as IN is promising. However, we caution that the current understanding of cirrus clouds, and especially the crucial process of ice nucleation, is currently inadequate, and any considerations of actual implementation of the CEM in question is therefore premature at this point. There are still several open questions regarding this CEM that need to be addressed, and further investigations are required. In conclusion, we here present a list of future studies needed to address outstanding issues that must be resolved in order to truly evaluate the viability of this CEM: (1) precise laboratory studies of the ice nucleating ability of BiI_3, as well as its toxicity and environmental fate; (2) sensitivity studies of cirrus clouds exploring the robustness of our findings to the subgrid-scale treatment of vertical velocities in cirrus clouds [see *Storelvmo et al.*, 2013]; (3) the implementation of the seeding material as a prognostic variable in climate simulations, in order to represent their full life cycle in the atmosphere, including emissions, ice nucleation in cirrus *and* mixed-phase clouds, as well as their removal rates via dry and wet deposition; (4) fully coupled climate simulations of the long-term climate

response to the CEM; and (5) detailed simulations of the distribution and transport of seeding material in the atmosphere, ideally with a particle dispersion model.

Acknowledgments
The work presented in this paper was supported in part by the facilities and staff of the Yale University Faculty of Arts and Sciences High Performance Computing Center.

References

Barahona, D., and A. Nenes (2008), Parameterization of cirrus cloud formation in large-scale models: Homogeneous nucleation, *J. Geophys. Res.*, *113*, D11211, doi:10.1029/2007JD009355.

Barahona, D., and A. Nenes (2009), Parameterizing the competition between homogeneous and heterogeneous freezing in ice cloud formation- polydisperse ice nuclei, *Atmos. Chem. Phys.*, *9*(5), 933–948, doi:10.5194/acp-9-5933-2009.

Budyko, M. I. (1969), The effect of solar radiation variations on the climate of the Earth, *Tellus*, *21*(5), 611–619, doi:10.1111/j.2153-3490.1969.tb00466.x.

Crutzen, P. J. (2006), Albedo enhancement by stratospheric sulfur injections: A contribution to resolve a policy dilemma?, *Clim. Change*, *77*(3–4), 211–220, doi:10.1007/s10584-006-9101-y.

Cziczo, D. J., K. D. Froyd, C. Hoose, E. J. Jensen, M. Diao, M. A. Zondlo, J. B. Smith, C. H. Twohy, and D. M. Murphy (2013), Clarifying the dominant sources and mechanisms of cirrus cloud formation, *Science*, *340*(6138), 1320–1324, doi:10.1126/science.1234145.

DeMott, P. J., D. J. Cziczo, A. J. Prenni, D. M. Murphy, S. M. Kreidenweis, D. S. Thomson, R. Borys, and D. C. Rogers (2003), Measurements of the concentration and composition of nuclei for cirrus formation, *PNAS*, *100*(25), 14,655–14,660, doi:10.1073/pnas.2532677100.

Gayet, J. F., J. Ovarlez, V. Shcherbakov, J. Strom, U. Schumann, A. Minikin, F. Auriol, A. Pethold, and M. Monier (2004), Cirrus cloud microphysical and optical properties at southern and northern midlatitudes during the INCA experiment, *J. Geophys. Res.*, *109*, D20206, doi:10.1029/2004JD004803.

Gettelman, A., X. Liu, S. J. Ghan, H. Morrison, S. Park, A. J. Conley, S. A. Klein, J. Boyle, D. L. Mitchell, and J. L. F. Li (2010), Global simulations of ice nucleation and ice supersaturation with an improved cloud scheme in the Community Atmosphere Model, *J. Geophys. Res.*, *115*, D18216, doi:10.1029/2009JD013797.

Haag, W., B. Kärcher, J. Ström, A. Minikin, U. Lohmann, J. Ovarlez, and A. Stohl (2003), Freezing thresholds and cirrus cloud formation mechanisms inferred from in situ measurements of relative humidity, *Atmos. Chem. Phys.*, *3*(5), 1791–1806, doi:10.5194/acp-3-1791-2003.

Koop, T., B. P. Luo, A. Tsias, and T. Peter (2000), Water activity as the determinant for homogeneous ice nucleation in aqueous solutions, *Nature*, *406*(6796), 611–614.

Lamarque, J. F., et al. (2010), Historical (1850–2000) gridded anthropogenic and biomass burning emissions of reactive gases and aerosols: Methodology and application, *Atmos. Chem. Phys.*, *10*, 7017–7039, doi:10.5194/acp-10-7017-2010.

Liu, X., et al. (2012a), Toward a minimal representation of aerosols in climate models: Description and evaluation in the Community Atmosphere Model CAM5, *Geosci. Model Dev.*, *5*, 709–739, doi:10.5194/gmd-5-709-2012.

Liu, X., X. Shi, K. Zhang, E. J. Jensen, A. Gettelman, D. Barahona, A. Nenes, and P. Lawson (2012b), Sensitivity studies of dust ice nuclei effect on cirrus clouds with the Community Atmosphere Model CAM5, *Atmos. Chem. Phys.*, *12*(24), 12,061–12,079, doi:10.5194/acp-12-12061-2012.

Mahowald, N. M., D. R. Mohs, S. Levis, P. J. Rasch, M. Yoshioka, C. S. Zender, and C. Luo (2006), Change in atmospheric mineral aerosols in response to climate: Last glacial period, preindustrial, modern, and doubled carbon dioxide climates, *J. Geophys. Res.*, *111*, D10202, doi:10.1029/2005JD006653.

Mitchell, D. L., and W. Finnegan (2009), Modification of cirrus clouds to reduce global warming, *Environ. Res. Lett.*, *4*(4), 045,102, doi:10.1088/1748-9326/4/4/045102.

Mitchell, D. L., S. Mishra, and R. P. Lawson (2011), Cirrus clouds and climate engineering: New findings on ice nucleation and theoretical basis, in *Planet Earth 2011—Global Warming Challenges and Opportunities for Policy and Practice*, vol. 12, edited by E. G. Caravannis, pp. 257–288, InTech., Rijeka, Croatia, doi:10.5772/902.

Morrison, H., and A. Gettelman (2008), A new two-moment bulk stratiform cloud microphysics scheme in the community atmosphere model, version 3 (CAM3). Part I: Description and numerical tests, *J. Clim.*, *21*, 3642–3659, doi:10.1175/2008jcli2105.1.

Prospero, J. M., P. Ginoux, O. Torres, S. E. Nicholson, and T. E. Gill (2002), Environmental characterization of global sources of atmospheric soil dust identified with the nimbus 7 total ozone mapping spectrometer (TOMS) absorbing aerosol product, *Rev. Geophys.*, *40*(1), 1002, doi:10.1029/2000RG000095.

Phillips, V. T. J., P. J. DeMott, and C. Andronache (2008), An empirical parameterization of heterogeneous ice nucleation for multiple chemical species of aerosol, *J. Atmos. Sci.*, *65*(9), 2757–2783, doi:10.1175/2007jas2546.1.

Rossow, W. B., and R. A. Schiffer (1999), Advances in understanding clouds from ISCCP, *Bull. Am. Meteorol. Soc.*, *80*(11), 2261–2287, doi:10.1175/1520-0477(1999).

Spichtinger, P., K. Gierens, and W. Read (2003), The global distribution of ice-supersaturated regions as seen by the Microwave Limb Sounder, *Q. J. R. Meteorolog. Soc.*, *129*(595), 3391–3410, doi:10.1256/qj.02.141.

Spichtinger, P., K. Gierens, H. G. J. Smit, J. Ovarlez, and J. F. Gayet (2004), On the distribution of relative humidity in cirrus clouds, *Atmos. Chem. Phys.*, *4*, 639–647, doi:10.5194/acp-4-639-2004.

Stephens, G. L. (2005), Cloud feedbacks in the climate system: A critical review, *J. Clim.*, *18*, 237–273.

Stephens, G. L., J. L. Li, M. Wild, C. A. Clayson, N. Loeb, S. Kato, T. L'Ecuyer, P. W. Stackhouse, M. Lebsock, and T. Andrews (2012), An update on Earth's energy balance in light of the latest global observations, *Nat. Geosci.*, *5*(10), 691–696, doi:10.1038/NGEO1580.

Storelvmo, T., J. E. Kristjansson, H. Muri, M. Pfeffer, D. Barahona, and A. Nenes (2013), Cirrus cloud seeding has potential to cool climate, *Geophys. Res. Lett.*, *40*(1), 178–182, doi:10.1029/2012GL054201.

Ström, J., et al. (2003), Cirrus cloud occurrence as function of ambient relative humidity: A comparison of observations from the Southern and Northern Hemisphere midlatitudes obtained during the INCA experiment, *Atmos. Chem. Phys.*, *3*, 1807–1816, doi:10.5194/acpd-3-3301-2003.

Welti, A., F. Lüönd, O. Stetzer, and U. Lohmann (2009), Influence of particle size on the ice nucleating ability of mineral dust, *Atmos. Chem. Phys.*, *9*, 6705–6715, doi:10.5194/acp-9-6705-2009.

Yu, H., L. A. Remer, M. Chin, H. Bian, Q. Tan, T. Yuan, and Y. Zhang (2012), Aerosols from Overseas Rival Domestic Emissions over North America, *Science*, *337*, 566–569, doi:10.1126/science.1217576.

Zelinka, M. D., S. A. Klein, K. E. Taylor, T. Andrews, M. J. Webb, J. M. Gregory, and P. M. Forster (2013), Contributions of different cloud types to feedbacks and rapid adjustments in CMIP5*, *J. Clim.*, *26*, 5007–5027, doi:10.1175/JCLI-D-12-00555.1.